Int. J. Solids Structures Vol. 30, No. 6, pp. 739–749, 1993
Printed in Great Britain

0020–7683/93 $6.00+ .00

INFINITE PERIODIC ARRAY OF CRACKS IN AXISYMMETRIC DISKING

S. SANTHANAM
Mechanical Engineering Department, Villanova University, Villanova, PA 19085, U.S.A.

(*Received* 22 *May* 1992; *in revised form* 15 *September* 1992)

Abstract—In axisymmetric disking, a periodic array of identical notches is placed on the surface of a brittle, cylindrical rod which is then encased in an elastic, annular sheath. Biaxial fluid pressure is applied to the composite and at a critical pressure cracks run across the diametral section of the rod producing a number of disks. The problem of multiple fracture is analysed using linear elastic fracture mechanics. A concentric circular cylinders model is assumed with perfect bonding at the interface. The flaws that initiate the fractures in the rod are modeled as an infinite periodic array of annular cracks perpendicular to the interface. The problem is formulated in terms of singular integral equations which are solved numerically. Stress intensity factors are obtained as a function of crack size, radius ratios and crack spacing for a glass rod–magnesium sheath combination. As the thickness of disks decreases pressures required for disking increase. The results presented here should also be of relevance to the problem of fiber fracture in a uniaxial fiber reinforced composite under biaxial compression.

1. INTRODUCTION

The phenomenon of disking was serendipitously discovered by Bridgman (1952). While trying to determine the biaxial compressive strength of glass by exposing sheathed glass rods to biaxial fluid pressure, he observed multiple fractures in the rod resulting in the formation of a number of thin disks. Jaeger and Cook (1963) observed a similar phenomenon while testing granite and other rock samples. In both instances, a brittle cylindrical rod is placed snug inside an annular elastic sheath. The exposed curved surface of the sheath is then subjected to fluid pressure. The applied pressure generates axial tensile stresses in the rod and compressive stresses in the sheath. Pre-existing natural flaws/cracks on the surface of the rod propagate across the section of the rod when the applied pressure exceeds a critical value. The possibility of utilizing this effect as a manufacturing process for cutting and slicing rods made of brittle materials such as glass, ceramics has been explored in the recent past (Santhanam, 1989; Nachi-Fujikoshi Corp., 1989). In both cases, flaws are deliberately placed at the desired locations of cuts. A commercial apparatus is now available that performs the process of disking on materials such as alumina, sapphire and glass.

The problem of fracture in disking has only been addressed in an empirical manner thus far. An analytical fracture criterion which predicts the effects of various geometric and material parameters on the fracture pressure can improve the design of the process. This paper is part of a systematic endeavour to analyse fracture in disking using linear-elastic fracture mechanics concepts. The case of a single crack in the rod was first considered (Santhanam, 1992). It was determined that the radius ratio and elastic modulus ratio have a strong influence on the stress intensity factors at the tip of the crack. This paper considers the case of multiple cracks in disking which is the normal mode in which the process is performed. The influence of crack spacing, as well as the other parameters mentioned above, on stress intensity factors is studied.

The problem of multiple cracks has been studied in a number of different geometries. Most studies deal with planar problems of a single, homogeneous, isotropic body. One of the earlier studies, by Lowengrub (1966), involved multiple parallel cracks in an infinite plane. Benthem and Koiter (1973) considered the case of a half plane with a periodic array of edge cracks using an asymptotic approximation method. Bowie (1973) tackled the same problem by a conformal mapping technique. Solutions for interacting arrays of parallel edge cracks subjected to thermal stress conditions have been developed by Nemat-Nasser

et al. (1978). Solutions have also been obtained for a periodic array of edge and internal cracks in a half plane subjected to arbitrary loading (Nied, 1987). Axisymmetric problems have also received some attention. Collins (1962) considered penny shaped cracks in an infinite elastic solid. A study that comes closest to the disking problem is that of Wijeye-wickrema and Keer (1992). Their problem was one of a fiber-reinforced brittle matrix composite under longitudinal tensile loading. A circular cylinders model was assumed with an infinite, parallel array of cracks in the matrix, perpendicular to the interface. Perfect bonding was assumed at the interface and solutions were obtained by the principle of superposition. A similar approach is used here for the disking problem. While the primary objective of this paper is to analyse fracture in the disking process, the results obtained here should also be of direct relevance to the problem of fiber fracture in uniaxial fiber-reinforced composites loaded in compression perpendicular to the fiber orientation.

2. PROBLEM FORMULATION

The axisymmetric disking geometry is modeled as two infinite concentric circular cylinders, with perfect bonding at the interface. The cylinders are isotropic, homogeneous and elastic. Henceforth, the subscripts/superscripts 1 and 2 refer to the rod and sheath respectively. The elastic moduli of the rod and sheath are E_1 and E_2, respectively, and the corresponding Poisson's ratios v_1 and v_2. The rod has an outer radius R_1 and the sheath an outer radius R_2. The periodic, annular edge cracks, that cause failure in the rod are perpendicular to the interface and of radial extent a with the inner crack tips at $r = c$, and the outer crack tips at $r = R_1$ ($a = R_1 - c$). The cracks are spaced a distance h apart along the z-axis. Loading is in the form of a uniform pressure p applied on the exposed cylindrical surface of the annular sheath (Fig. 1).

The required solution is obtained by the superposition of two related problems. In the first problem the concentric cylinders, in the absence of cracks, are subjected to the external pressure. The solution to this problem can be found in Santhanam (1992). In the second problem the concentric cylinder model is considered with multiple cracks in the rod and

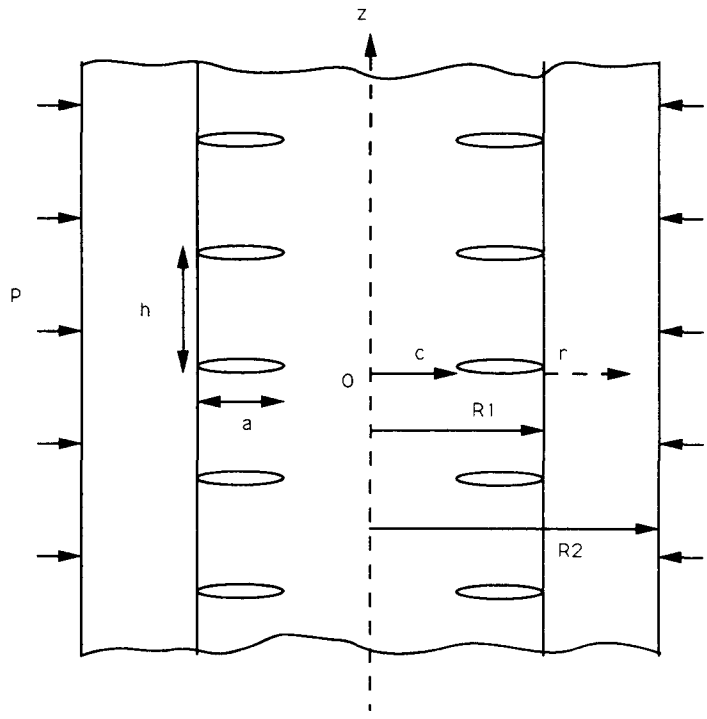

Fig. 1. Concentric circular cylinders model with multiple cracks in inner cylinder.

loading in the form of crack surface tractions. Crack surface tractions in the second problem are equal and opposite to the longitudinal stresses (σ_z^1) obtained as the solution in the first problem. The second problem of multiple cracks is solved by making use of the stress field solution for a single crack (Santhanam, 1992).

Only one half of the disking geometry ($z \geqslant 0$) is considered because of symmetry. Since both the geometry and loading are axially symmetric, the non-zero displacement and stress components can be expressed in terms of Love's axisymmetric biharmonic stress function $\chi(r, z)$. For the rod, Love's stress function is as follows (Wijeyewickrema and Keer, 1991):

$$\chi^1(r,z) = \frac{2}{\pi}\int_0^\infty [f_1(s)I_0(rs) + f_2(s)rsI_1(rs)] \sin(zs)\,\mathrm{d}s + \int_0^\infty f_3(p)p(2\nu_1 + zp)\,\mathrm{e}^{-zp} J_0(rp)\,\mathrm{d}p. \quad (1)$$

Love's stress function for the sheath region is:

$$\chi^2(r,z) = \frac{2}{\pi}\int_0^\infty [f_4(s)I_0(rs) + f_5(s)rsI_1(rs) + f_6(s)K_0(rs) + f_7(s)rsK_1(rs)] \sin(zs)\,\mathrm{d}s + \int_0^\infty f_8(p)p(2\nu_2 + zp)\,\mathrm{e}^{-zp} J_0(rp)\,\mathrm{d}p, \quad (2)$$

where the functions $f_i(s)$, $(i = 1, 2, \ldots, 8)$ are to be determined, $J_n(\ )$ are the Bessel functions of the first kind of order n, $I_n(\ )$ and $K_n(\ )$ are the modified Bessel's function of the first and second kind, respectively, of order n. μ_1 and μ_2 are the shear moduli of the rod and sheath respectively. The radial displacement u_r, axial displacement u_z, radial stress (σ_r), tangential stress σ_θ, axial stress σ_z, and shear stress σ_{rz} in the rod and sheath can be obtained from their respective stress functions using:

$$u_r(r,z) = -\frac{1}{2\mu}\frac{\partial^2\chi}{\partial r\,\partial z}, \quad (3)$$

$$u_z(r,z) = \frac{1}{2\mu}\left[2(1-\nu)\nabla^2\chi - \frac{\partial^2\chi}{\partial z^2}\right], \quad (4)$$

$$\sigma_r(r,z) = \frac{\partial}{\partial z}\left[\nu\nabla^2\chi - \frac{\partial^2\chi}{\partial r^2}\right], \quad (5)$$

$$\sigma_\theta(r,z) = \frac{\partial}{\partial z}\left[\nu\nabla^2\chi - \frac{1}{r}\frac{\partial\chi}{\partial r}\right], \quad (6)$$

$$\sigma_z(r,z) = \frac{\partial}{\partial z}\left[(2-\nu)\nabla^2\chi - \frac{\partial^2\chi}{\partial z^2}\right], \quad (7)$$

$$\sigma_{rz} = \frac{\partial}{\partial r}\left[(1-\nu)\nabla^2\chi - \frac{\partial^2\chi}{\partial z^2}\right], \quad (8)$$

where, $\chi(r, z)$ is the appropriate axisymmetric biharmonic function, ∇^2 is the axisymmetric Laplacian operator, and ν is the Poisson's ratio. The complete displacement and stress fields for the rod and sheath can be found in Santhanam (1992) and Wijeyewickrema and Keer (1991). In particular the axial stress $\sigma_z^1(r, z)$ in the rod is given by:

$$\sigma_z^1(r,z) = \frac{2}{\pi}\int_0^\infty \{f_1(s)I_0(rs) + f_2(s)[2(2-\nu_1)I_0(rs) + rsI_1(rs)]\}s^3 \cos(zs)\,ds + \int_0^\infty f_3(p)p^4(1+zp)\,e^{-zp}\,J_0(rp)\,dp, \quad (9)$$

where ν_1 is the Poisson's ratio of the rod material.

The boundary conditions at the interface are derived from the perfect bonding that is assumed between the rod and sheath.

$$u_r^1(R_1,z) = u_r^2(R_1,z) \quad u_z^1(R_1,z) = u_z^2(R_1,z) \quad 0 \leqslant z < \infty. \quad (10)$$

$$\sigma_r^1(R_1,z) = \sigma_r^2(R_1,z) \quad \sigma_{rz}^1(R_1,z) = \sigma_{rz}^2(R_1,z) \quad 0 \leqslant z < \infty. \quad (11)$$

The boundary conditions on the external cylindrical surface of the sheath are:

$$\sigma_r^2(R_2,z) = 0, \quad \sigma_{rz}^2(R_2,z) = 0, \quad 0 \leqslant z < \infty. \quad (12)$$

On the planes of symmetry, $z = nh$ $(n = -\infty, \cdots, +\infty)$, the appropriate conditions are:

$$\sigma_{rz}^1(r,nh) = 0, \quad 0 \leqslant r \leqslant R_1, \quad \sigma_{rz}^2(r,nh) = 0, \quad R_1 \leqslant r \leqslant R_2, \quad (13)$$

$$\sigma_z^1(r,nh) = -\sigma(r), \quad c < r < R_1, \quad (14)$$

$$u_z^1(r,nh) = 0, \quad 0 \leqslant r < c, \quad u_z^2(r,nh) = 0, \quad R_1 < r \leqslant R_2. \quad (15)$$

Here $\sigma(r)$ is the axial stress obtained from the first problem, $r = c$ represents the inner tip of the annular crack where $c = (R_1 - a)$.

It can be easily shown that eqn (13) is satisfied by the forms assumed for the shear stresses. From the second part of eqn (15) it can be shown that $f_8(p)$ is identically zero. The problem can now be expressed in the form of an integral equation by introducing a new unknown function $G(r)$ which is related to the gradient of the crack opening displacement:

$$\frac{\mu_1}{1-\nu_1}\frac{\partial}{\partial r}u_z^1(r,0) = G(r). \quad (16)$$

From eqn (16), the first part of eqn (15) (for $n = 0$), and the expression for u_z^1 (as a function of f_1, f_2 and f_3), the following relation can be obtained:

$$p^3 f_3(p) = \int_c^{R_1} tG(t)J_1(pt)\,dt. \quad (17)$$

A system of six equations relating the unknown functions f_i, $(i = 1, 2, 4, 5, 6, 7)$ are obtained (Appendix) from the boundary conditions at the interface [eqns (10) and (11)] and the external surface of the sheath [eqn (12)]. The system of six equations can be solved for the unknown functions f_i $(i = 1, 2, 4, 5, 6, 7)$:

$$f_i(s) = \frac{1}{s^3}\int_c^{R_1} tG(t)\,dt \sum_{j=1}^{4} \frac{A_{ij}(s)h_j(t,s)}{\Delta(s)}, \quad (18)$$

where $\Delta(s)$ is the determinant and $A_{ij}(s)$ $[i = 1, 2, 4, 5, 6, 7; j = 1, \ldots, 6]$ are the appropriate elements of the adjoint of the coefficient matrix of the system of equations [eqns (A1)–(A6)] in the Appendix. The functions $h_j(t,s), j = 1, \ldots, 4$, are also defined in the Appendix

[eqns (A7)–(A10)]. Substituting for f_i, $(i = 1, 2, 3)$, from eqns (17) and (18), in eqn (9), the axial stress $\sigma_z^1(r, z)$ at any location in the upper half of the rod due to a single crack located at $z = 0$, is:

$$\sigma_z^1(r,z) = \frac{2}{\pi}\int_c^{R_1} tG(t)\,dt \int_0^\infty \overline{k_2}(r,t,s)\cos(zs)\,ds + \int_c^{R_1} tM(r,t,z)G(t)\,dt, \tag{19}$$

where

$$\overline{k_2}(r,t,s) = \frac{1}{\Delta(s)}\left\{I_0(rs)\sum_{j=1}^{4} A_{1j}h_j + [2(2-\nu_1)I_0(rs) + rsI_1(rs)]\sum_{j=1}^{4} A_{2j}h_j\right\} \tag{20}$$

and

$$M(r,t,z) = \frac{1}{t\pi T_1^{1/2}}\left\{\frac{E(k)}{T_2}\left[(t^2-r^2-z^2) + \frac{z^2[(t^2-r^2)(7t^2+r^2)+z^2(6t^2-2r^2-z^2)]}{T_1T_2}\right] + K(k)\left[1-\frac{z^2(t^2-r^2-z^2)}{T_1T_2}\right]\right\}. \tag{21}$$

Here,

$$T_1 = (t+r)^2+z^2, \quad T_2 = (t-r)^2+z^2, \quad k^2 = \frac{4tr}{T_1}, \tag{22}$$

and $K(k)$ and $E(k)$ are complete elliptic integrals of the first and second kind respectively.

Using the principle of superposition, the axial stress in the rod on the $z = 0$ plane due to the cracks located in the upper part of the rod $(z > 0)$ is obtained from eqn (19) by setting $z = nh$ and summing on n from $+1$ to ∞. From symmetry considerations the axial stress in the rod on the $z = 0$ plane due to cracks located in the lower part of the cylinder $(z < 0)$ is the same as the effect of the cracks located in the upper half of the rod. Hence the axial stress $\sigma_z^{1a}(r, 0)$ on the $z = 0$ plane due to all the cracks except the central crack (located on the $z = 0$ plane) is:

$$\sigma_z^{1a}(r,0) = 2\int_c^{R_1} tG(t)K_2(r,t)\,dt, \tag{23}$$

where

$$K_2(r,t) = \frac{2}{\pi}\int_0^\infty \overline{k_2}(r,t,s)\sum_{n=1}^{\infty}\cos(nhs)\,ds + \sum_{n=1}^{\infty} M(r,t,nh). \tag{24}$$

The axial stress $\sigma_z^{1b}(r, 0)$ on the $z = 0$ plane due to the central crack is

$$\sigma_z^{1b}(r,0) = \frac{1}{\pi}\int_c^{R_1}\left\{\frac{1}{t-r} + L(r,t)\right\}G(t)\,dt, \tag{25}$$

where

$$L(r,t) = L_1(r,t) + 2tL_2(r,t), \tag{26}$$

$$L_1(r,t) = \frac{m(r,t)-1}{t-r} + \frac{m(r,t)}{t+r}, \tag{27}$$

$$m(r,t) = \begin{cases} E\left(\frac{r}{t}\right), & r < t, \\ \frac{r}{t}E\left(\frac{t}{r}\right) + \frac{t^2-r^2}{rt}K\left(\frac{t}{r}\right), & r > t, \end{cases} \tag{28}$$

$$L_2(r,t) = \int_0^\infty \overline{k_2}(r,t,s)\,\mathrm{d}s. \tag{29}$$

The axial stress on the $z = 0$ plane due to all the cracks is

$$\sigma_z^1(r,0) = \frac{1}{\pi}\int_c^{R_1}\left\{\frac{1}{t-r} + L(r,t) + 2\pi t K_2(r,t)\right\}G(t)\,\mathrm{d}t. \tag{30}$$

The required integral equation is then obtained from eqns (14) and (30) as:

$$\frac{1}{\pi}\int_c^{R_1}\left\{\frac{1}{t-r} + L(r,t) + 2\pi t K_2(r,t)\right\}G(t)\,\mathrm{d}t = -\sigma(r), \quad c < r < R_1. \tag{31}$$

The outer crack tip at $r = R_1$, on the $z = 0$ plane, is located at the interface. As a consequence, $L_2(r,t)$ is not bounded for all r, t in the closed interval $[c, R_1]$. Hence, the singularity in the solution at this point is not of the usual square root type. Erdol and Erdogan (1978) have developed a method for dealing with such kernels. The asymptotic value of the integrand in eqn (29) is first added and subtracted from itself. $L_2(r,t)$ can then be expressed as

$$L_2(r,t) = L_{2f}(r,t) + L_{2s}(r,t), \tag{32}$$

where L_{2f} is bounded in the closed interval and L_{2s} becomes unbounded as r and t approach the end point $r, t = R_1$. After some manipulations the singular part, L_{2s} can be shown to be:

$$L_{2s}(r,t) = \frac{1}{2\sqrt{rt}}\left\{\frac{c_0}{(2R_1-r-t)} - \frac{c_1(R_1-r)}{(2R_1-r-t)^2} + \frac{2c_2(R_1-r)^2}{(2R_1-r-t)^3}\right\}, \tag{33}$$

$$c_0 = \frac{1}{2}\left[1 - \frac{m(1+\kappa_1)}{m+\kappa_2} - \frac{3(1-m)}{1+m\kappa_1}\right], \quad c_1 = -\frac{6(1-m)}{1+m\kappa_1}, \quad c_2 = -\frac{2(1-m)}{1+m\kappa_1}, \quad m = \frac{\mu_2}{\mu_1}, \tag{34}$$

where $\kappa_i = 3-4\nu_i$, $(i = 1, 2)$. The singular kernal in eqn (33) is essentially the same as the expressions found for the corresponding plane strain problem considered in Erdogan *et al.* (1973). The integral equation (31) thus has a generalized Cauchy kernel. The following solution form is assumed (Erdogan *et al.*, 1973):

$$G(t) = (R_1-t)^\beta(t-c)^\alpha\psi(t), \quad c < t < R_1. \tag{35}$$

The characteristic equations required to determine α and β are given by:

$$\cot(\pi\alpha) = 0, \tag{36}$$

$$2d_1 \cos(\pi\{\beta+1\}) - d_2(\beta+1)^2 - d_3 = 0, \tag{37}$$

where

$$d_1 = (m+\kappa_2)(1+m\kappa_1), \tag{38}$$

$$d_2 = -4(m+\kappa_2)(1-m), \tag{39}$$

$$d_3 = (1-m)(m+\kappa_2)+(1+m\kappa_1)(m+\kappa_2)-m(1+\kappa_1)(1+m\kappa_1). \tag{40}$$

Since the inner crack tip is embedded in a homogeneous medium, eqn (36) gives the usual $\alpha = -1/2$ singularity. Equation (37) is solved numerically to determine the constant β. Using a change of variables the interval (c, R_1) is normalized:

$$t = \frac{R_1-c}{2}\tau + \frac{R_1+c}{2}, \quad r = \frac{R_1-c}{2}\rho + \frac{R_1+c}{2}, \tag{41}$$

$$G(t) = (1-\tau)^{\beta}(\tau+1)^{\alpha}g(\tau), \tag{42}$$

$$H(\rho,\tau) = \frac{R_1-c}{2}\{L(r,t)+2\pi t K_2(r,t)\}, \tag{43}$$

$$\sigma(r) = \Sigma(\rho). \tag{44}$$

Equation (31) can now be expressed as

$$\frac{1}{\pi}\int_{-1}^{+1}\left\{\frac{1}{\tau-\rho}+H(\rho,\tau)\right\}g(\tau)(1-\tau)^{\beta}(\tau+1)^{\alpha}\,d\tau = -\Sigma(\rho), \quad -1<\rho<+1. \tag{45}$$

This equation has to be solved along with the crack closure condition

$$\int_{-1}^{+1} g(\tau)(1-\tau)^{\beta}(\tau+1)^{\alpha}\,d\tau = 0. \tag{46}$$

The singular integral equation with a generalized Cauchy kernal [eqn (45)] along with the crack closure condition (46) is solved using a Gauss–Jacobi integration formula. Details of this formula can be found in Erdogan *et al.* (1973). The quantity of interest in this analysis is the stress intensity factor at the crack tips $r = c$. The mode I stress intensity factor at this tip is defined by:

$$k_1(c) = \lim_{r\to c}\sqrt{2(c-r)}\,\sigma_z^1(r,0), \tag{47}$$

which can be expressed as

$$k_1(c) = -2^{\beta}(R_1-c)^{1/2}g(-1). \tag{48}$$

(R_1-c) represents the crack length a. The formulae given by Krenk (1975) are used to obtain $g(-1)$.

3. RESULTS AND DISCUSSION

In the disking process, the quantity of principal interest is the stress intensity factor (k_I) at the inner crack tip ($r = c$). Stress intensity factors are computed using the approach outlined above and are non-dimensionalized in the following manner:

$$Y(c) = \frac{k_I(c)}{p\sqrt{a}} = -2^{\beta} g(-1). \tag{49}$$

The non-dimensional stress intensity factor $Y(c)$ is influenced by the radius ratio (R_2/R_1), the elastic modulus ratio (E_2/E_1), the Poisson's ratios ν_1 and ν_2, and the crack spacing (h/a). The effects of the radius ratio (R_2/R_1) and the elastic modulus ratio (E_2/E_1) on $Y(c)$ for an isolated crack have been reported previously (Santhanam, 1992). As the radius ratio (R_2/R_1) increases the tensile stress induced in the rod by the applied pressure increases and as a consequence so does k_I. A similar effect is observed when the ratio E_2/E_1 decreases. It is also observed that $Y(c)$ increases as the crack size (a/R_1) increases. The parameter of interest in this paper is the crack spacing (h/a) and its influence on the stress intensity factor ($Y(c)$) at the inner crack tip.

The viability of axisymmetric disking has been established experimentally with glass as the specimen material (Santhanam, 1989). Glass rods, of diameter ranging from 6 to 12 mm, encased in sheaths of magnesium and acetal have been cut into disks of thickness ranging from 3 to 6 mm. Figures 2 and 3 show non-dimensional stress intensity factors for a glass–magnesium composite as a function of crack spacing (h/a), crack size (a/R_1), and radius ratio (R_2/R_1). Glass has an elastic modulus of 69 GPa (10.0E6 psi) with a Poisson's ratio of 0.23. The corresponding values for magnesium are 35 GPa (5.0E6 psi) and 0.30 respectively. The parameter m for this material combination is 0.48. In Fig. 2, the non-dimensional stress intensity factors, $Y(c)$, have been determined for $R_2/R_1 = 1.5$. For a given crack length (a/R_1), $Y(c)$ increases as the crack spacing increases. For crack spacings (h/a) greater than 5.0, the change in $Y(c)$ with (h/a) is very small and $Y(c)$ asymptotically tends to the value corresponding to an isolated crack, i.e. infinite crack spacing. For example, $Y(c)$ is 0.186 for a crack spacing $h/a = 10.0$ ($a/R_1 = 0.1$; $R_2/R_1 = 1.5$). $Y(c)$ for an isolated crack (infinite h/a) is 0.187 for an otherwise identical geometry. The non-dimensionalized factors also increase with crack length, for a fixed (R_2/R_1) and (h/a), due to the diminishing influence of the interface on the inner crack tip. Only three different crack lengths were considered here ((a/R_1) = 0.1, 0.2, 0.3). Solutions for larger crack lengths can also be obtained, but were not considered because initial crack lengths used in disking never exceed $0.25R_1$. Moreover the effect of crack length on $Y(c)$ is readily apparent from these three crack sizes (Fig. 2). Figure 3 is similar to Fig. 2 except that the radius ratio (R_2/R_1) is 2.5. The larger radius ratio results in higher $Y(c)$ values but all other trends remain the same.

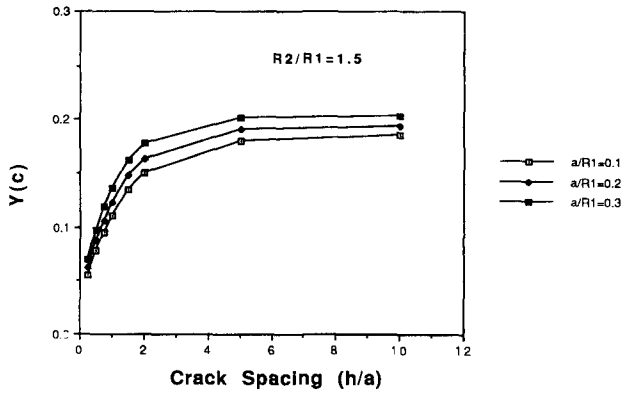

Fig. 2. Non-dimensional stress intensity factors as a function of crack spacing for the disking of glass rods in a magnesium sheath ($R_2/R_1 = 1.5$).

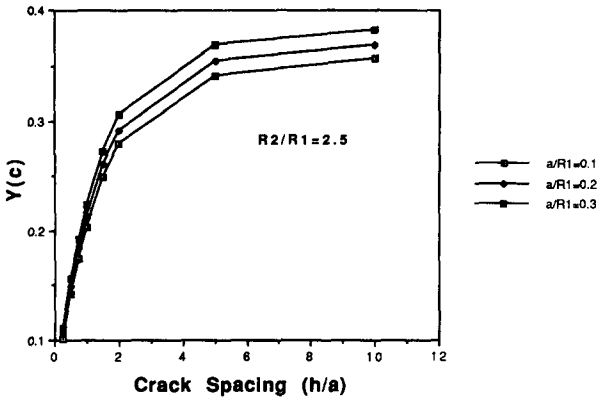

Fig. 3. Non-dimensional stress intensity factors as a function of crack spacing for a glass–magnesium combination ($R_2/R_1 = 2.5$).

Besides the crack tip at $r = c$, there is another crack tip at the interface ($r = R_1$). The stress intensity factor at this tip, $k_1(R_1)$, is defined as:

$$k_1(R_1) = \lim_{r \to R_1} 2^{1/2}(r - R_1)^{-\beta}\sigma_z^2(r, 0). \tag{50}$$

For the glass–magnesium material combination, the singularity parameter $\beta = -0.5684$. Stress intensity factors at the interface tip can be and were computed for all parameter combinations considered in Figs 2 and 3. In all cases, $k_1(R_1)$ is smaller than $k_1(c)$, but this comparison is invalid because the strengths of the singularities at the two tips are different (-0.5 versus -0.5684). For the glass–magnesium combination, the inner crack tip ($r = c$) is more critical because the fracture toughness of glass is a lot less than that of magnesium. Experimentally, failure always occurs from the inner tip and never from the interface tip. There is also the possibility of debonding at the interface at and around the interface tip which could potentially reduce the stess intensity factors at both tips. However, this phenomenon is not considered in this paper and perfect bonding is assumed to exist at the interface.

A few words about the numerical accuracy of the results in Figs 2 and 3 would be in order here. The Gauss–Jacobi method used to solve eqns (45) and (46) involves expanding the function $g(\tau)$ as an infinite series of Jacobi polynomials. For purposes of numerical computation, this series is truncated to typically 20 terms. There is also a truncation involved in the infinite series in $K_2(r, t)$ [eqn (24)]. The truncation number (N) here depends on the crack spacing ratio (h/a). The larger the value of (h/a) the smaller the trunction number, N. N ranges from 10 for (h/a) = 5 and greater, to 300 for (h/a) = 0.1. Convergence is considered to be achieved if the change in $Y(c)$ is less than 0.5% for a 10% increase in the truncation numbers.

These results have implications for the pressures required for disking. Fracture, in disking, initiates at the flaws that are introduced on the surface of the specimens. These flaws are typically introduced using a loaded indentor as in a hardness tester. Flaw sizes usually range from 0.25 to 1.0 mm. With glass, thickness of disks produced range from 3 to 6 mm giving a crack spacing ratio (h/a) of 3 and above. For these ratios the influence of neighboring cracks on the crack tip k_1 is small. It is envisioned that the disking process will be used for producing wafers of thickness 1 mm or less. In this regime, results indicate that there will be a strong influence of crack spacing on pressure required for fracture.

As indicated earlier, the results of this analysis would also be applicable to fiber-reinforced composites. When a unidirectional fiber-reinforced composite is subjected to compressive stresses applied perpendicular to the fiber axes (as in Fig. 1), the mismatch in axial Poisson's extension will create axial stresses in both the matrix and the fibers. These axial stresses will be tensile in the fibers when the fibers are stiffer than the matrix which is

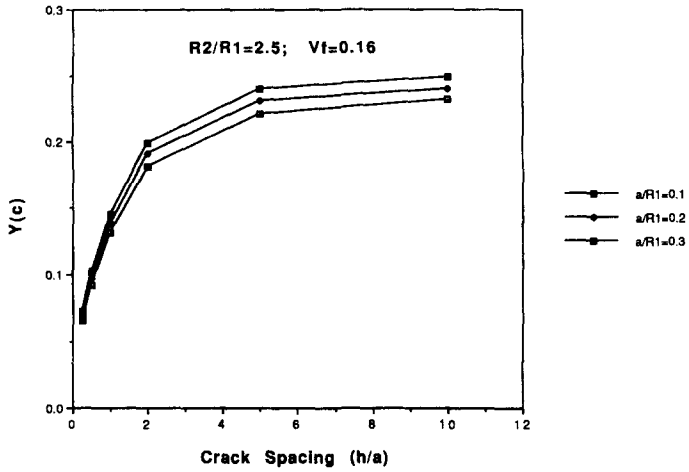

Fig. 4. Non-dimensional stress intensity factors for a CAS/SiC composite ($R_2/R_1 = 2.5$, $V_f = 0.16$).

usually the case. Axial tensile stresses can also arise in the fibers when a mismatch in thermal expansion arises due to a uniform temperature increase. In either event, fibers can fail thus reducing the load carrying capacity of the composite. In Fig. 4 results [$Y(c)$] are presented for a composite comprised of a calcium aluminosilicate glass ceramic matrix reinforced with silicon carbide fibers (SiC/CAS). This composite was considered by Wijeyewickrema and Keer (1991, 1992) in their studies related to matrix cracking in a composite. CAS has an elastic modulus of 98 GPa and a Poisson's ratio of 0.25. The corresponding numbers for SiC are 207 GPa and 0.25 respectively. The parameter m is 0.472 and the singularity parameter $\beta = -0.5816$ for this material combination. The radius ratio assumed is 2.5 which corresponds to a volume fraction of 0.16 for the composite. $Y(c)$ values are shown in Fig. 4 as a function of crack spacing and crack size. Clearly crack interaction effects are significant when crack spacing is of the order of crack size in the fibers. This would be true for the interface crack tip too. For the SiC/CAS material combination, fracture could initiate at either crack tip. Where fracture initiates will depend on the geometrical parameters as well as the toughness of the two materials and in particular the toughness at the interface. Debonding is a distinct possibility and this in turn will affect the stress intensity factors.

REFERENCES

Benthem, J. P. and Koiter, W. T. (1973). Asymptotic approximations to crack problems. In *Mechanics of Fracture I: Methods of Analysis and Solutions of Crack Problems* (Edited by G. C. Sih), pp. 131–178. Noordhoff, Leyden.

Bowie, O. L. (1973). Solutions of plane crack problems by mapping technique. In *Mechanics of Fracture I: Methods of Analysis and Solutions of Crack Problems* (Edited by G. C. Sih), pp. 1–55. Noordhoff, Leyden.

Bridgman, P. W. (1952). *The Physics of High Pressure*. G. Bell and Sons, London.

Collins, W. D. (1962). Some axially symmetric stress distributions in elastic solids containing penny shaped cracks. *Proc. R. Soc. Lond.*, Series A, **266**, 359–386.

Erdogan, F., Gupta, G. D. and Cook, T. S. (1973). Numerical solution of singular integral equations. In *Mechanics of Fracture I: Methods of Analysis and Solution of Crack Problems* (Edited by G. C. Sih), pp. 368–425. Noordhoff, Leyden.

Erdol, R. and Erdogan, F. (1978). A thick-walled cylinder with an axisymmetric internal or edge crack. *ASME J. Appl. Mech.* **45**, 281–286.

Jaeger, J. C. and Cook, N. G. W. (1963). Pinching-off and disking of rocks. *J. Geophys. Res.* **68**(6), 1759–1782.

Krenk, S. (1975). On the use of the interpolation polynomial for solutions of singular integral equations. *Q. Appl. Math.* **32**, 479–484.

Lowengrub, M. (1966). A two dimensional crack problem. *Int. J. Engng Sci.* **4**, 289–298.

Nachi-Fujikoshi Corp. (1989). Super high lateral pressure cutting machine. Nachi Catalog No. H1051E.

Nemat-Nasser, S., Keer, L. M. and Parihar, K. S. (1978). Unstable growth of thermally induced interacting cracks in brittle solids. *Int. J. Solids Structures* **14**, 409–430.

Nied, H. F. (1987). Periodic array of cracks in a half plane subjected to arbitrary loading. *ASME J. Appl. Mech.* **54**, 642–648.

Santhanam, S. (1989). The precision crack-off process. Ph.D. Dissertation, Arizona State University, Tempe.

Santhanam, S. (1992). Fracture criterion for the axisymmetric disking process. *Int. J. Fract.* (accepted).

Wijeyewickrema, A. C. and Keer, L. M. (1991). Matrix fracture in brittle matrix fiber-reinforced composites. *Int. J. Solids Structures* **28**(1), 43–65.

Wijeyewickrema, A. C. and Keer, L. M. (1992). Matrix crack interaction in a fiber-reinforced brittle matrix composite. *Int. J. Solids Structures* **29**(5), 559–570.

APPENDIX

The four continuity conditions at the interface of the cylinders and the two traction-free conditions on the external surface of the outer cylinder are:

$$f_1(s)I_1(R_1s)+f_2(s)R_1sI_0(R_1s)-\mu f_4(s)I_1(R_1s)-\mu f_5(s)R_1sI_0(R_1s)$$
$$+\mu f_6(s)K_1(R_1s)+\mu f_7(s)R_1sK_0(R_1s)=\frac{1}{s^3}\int_c^{R_1} tG(t)h_1(t,s)\,dt, \quad \text{(A1)}$$

$$f_1(s)I_0(R_1s)+f_2(s)[4(1-\nu_1)I_0(R_1s)+R_1sI_1(R_1s)]-\mu f_4(s)I_0(R_1s)$$
$$-\mu f_5(s)[4(1-\nu_2)I_0(R_1s)+R_1sI_1(R_1s)]-\mu f_6(s)K_0(R_1s)$$
$$-\mu f_7(s)[-4(1-\nu_2)K_0(R_1s)+R_1sK_1(R_1s)]=\frac{1}{s^3}\int_c^{R_1} tG(t)h_2(t,s)\,dt, \quad \text{(A2)}$$

$$f_1(s)\left[-I_0(R_1s)+\frac{I_1(R_1s)}{R_1s}\right]+f_2(s)[(2\nu_1-1)I_0(R_1s)-R_1sI_1(R_1s)]-f_4(s)\left[-I_0(R_1s)+\frac{I_1(R_1s)}{R_1s}\right]$$
$$+f_5(s)[(1-2\nu_2)I_0(R_1s)+R_1sI_1(R_1s)]+f_6(s)\left[K_0(R_1s)+\frac{K_1(R_1s)}{R_1s}\right]$$
$$-f_7(s)[(1-2\nu_2)K_0(R_1s)-R_1sK_1(R_1s)]=\frac{1}{s^3}\int_c^{R_1} tG(t)h_3(t,s)\,dt, \quad \text{(A3)}$$

$$f_1(s)I_1(R_1s)+f_2(s)[R_1sI_0(R_1s)+2(1-\nu_1)I_1(R_1s)]-f_4(s)I_1(R_1s)-f_5(s)$$
$$\times[R_1sI_0(R_1s)+2(1-\nu_2)I_1(R_1s)]+f_6(s)K_1(R_1s)$$
$$+f_7(s)[R_1sK_0(R_1s)-2(1-\nu_2)K_1(R_1s)]=\frac{1}{s^3}\int_c^{R_1} tG(t)h_4(t,s)\,dt, \quad \text{(A4)}$$

$$f_4(s)\left[-I_0(R_2s)+\frac{I_1(R_2s)}{R_2s}\right]-f_5(s)[(1-2\nu_2)I_0(R_2s)+R_2sI_1(R_2s)]$$
$$-f_6(s)\left[K_0(R_2s)+\frac{K_1(R_2s)}{R_2s}\right]+f_7(s)[(1-2\nu_2)K_0(R_2s)-R_2sK_1(R_2s)]=0, \quad \text{(A5)}$$

$$f_4(s)I_1(R_2s)+f_5(s)[R_2sI_0(R_2s)+2(1-\nu_2)I_1(R_2s)]$$
$$-f_6(s)K_1(R_2s)+f_7(s)[-R_2sK_0(R_2s)+2(1-\nu_2)K_1(R_2s)]=0, \quad \text{(A6)}$$

where $\mu=(\mu_1/\mu_2)$, and $h_i(t,s)$ are as given below:

$$h_1(t,s)=s\{-tsI_0(ts)K_1(R_1s)+R_1sI_1(ts)K_0(R_1s)+2(1-\nu_1)I_1(ts)K_1(R_1s)\}, \quad \text{(A7)}$$

$$h_2(t,s)=s\{tsK_0(R_1s)I_0(ts)+2(1-\nu_1)K_0(R_1s)I_1(ts)-R_1sK_1(R_1s)I_1(ts)\}, \quad \text{(A8)}$$

$$h_3(t,s)=-s\{I_1(ts)K_1(R_1s)\left[\frac{2(\nu_1-1)}{R_1s}-R_1s\right]+tsI_0(ts)K_0(R_1s)-I_1(ts)K_0(R_1s)+\frac{t}{R_1}I_0(ts)K_1(R_1s)\}, \quad \text{(A9)}$$

$$h_4(t,s)=s\{-tsI_0(ts)K_1(R_1s)+R_1sI_1(ts)K_0(R_1s)\}. \quad \text{(A10)}$$